Heliyon 10 (2024) e31889

Contents lists available at ScienceDirect

Heliyon

journal homepage: www.cell.com/heliyon

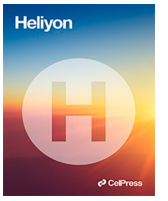

Research article

Diagnostic efficacy of complexity metrics from cardiac MRI myocardial segmental motion curves in detecting late gadolinium enhancement in myocardial infarction patients

Geng Li [a,b,1], Chong Zheng [a,b,1], Yadong Cui [a,b], Jin Si [c], Yang Yang [d], Jing Li [c], Jie Lu [a,b,*]

[a] Department of Radiology and Nuclear Medicine, Xuanwu Hospital, Capital Medical University, Beijing, China
[b] Beijing Key Laboratory of Magnetic Resonance Imaging and Brain Informatics, Beijing, China
[c] Department of Geriatrics, Xuanwu Hospital, Capital Medical University, National Clinical Research Center for Geriatric Diseases, Beijing, China
[d] Beijing United Imaging Research Institute of Intelligent Imaging, Beijing, China

ARTICLE INFO

Keywords:
Cardiovascular magnetic resonance imaging
Complexity metrics
Late gadolinium enhancement
Segmental myocardial strain

ABSTRACT

Background: Myocardial segmental motion is associated with cardiovascular pathology, often assessed through myocardial strain features. The stability of the motion can be influenced by myocardial fibrosis. This research aimed to explore the complexity metrics (CM) of myocardial segmental motion curves, observe their correlation with late gadolinium enhancement (LGE) transmural extension (TE), and assess diagnostic efficacy combined with segmental strains in different TE segments.

Methods: We included 42 myocardial infarction patients, dividing images into 672 myocardial segments (208 remote, 384 viable, and 80 unviable segments based on TE). Radial and circumferential segmental strain, along with CM for motion curves, were extracted. Correlation between CM and LGE, as well as the potential distinguishing role of CM, was evaluated using Pearson correlation, univariate linear regression (F-test), multivariate regression analysis (T-test), area under curve (AUC), machine learning models, and DeLong test.

Results: All CMs showed significant linear correlation with TE ($P < 0.001$). Six CMs were correlated with TE ($r > 0.3$), with radial frequency drift (FD) displayed the strongest correlation ($r = 0.496$, $P < 0.001$). Radial and circumferential FD significantly differed in higher TE myocardium than in remote segments ($P < 0.05$). Radial FD had practical diagnostic efficacy (remote vs. unviable AUC = 0.89, viable vs. unviable AUC = 0.77, remote vs. viable AUC = 0.65). Combining CM with segmental strain features boosted diagnostic efficacy than models using only segmental strain features (DeLong test, $P < 0.05$).

Abbreviations: **ACC**, accuracy; **AUC**, area under curve; **CM**, complexity metrics; **CMR**, cardiac magnetic resonance; **FD**, frequency drift; **LGE**, late gadolinium enhancement; **LV**, left ventricle; **ROC**, receiver operating characteristic; **Sens**, sensitivity; **Spec**, specificity; **SVM**, support vector machine; **TE**, transmural extension; **XGBoost**, eXtreme Gradient Boosting models.

* Corresponding author. Department of Nuclear Medicine, Xuanwu Hospital, Capital Medical University, No. 45 Changchun Street, Xicheng District, 100053, Beijing, China.

E-mail addresses: regan1995@foxmail.com (G. Li), 17812089921@163.com (C. Zheng), cyd1130@163.com (Y. Cui), sijinfirst@163.com (J. Si), yang.yang03@cri-united-imaging.com (Y. Yang), shpxbb@sina.com (J. Li), imaginglu@hotmail.com (J. Lu).

[1] Geng Li and Chong Zheng contributed equally to this work.

https://doi.org/10.1016/j.heliyon.2024.e31889
Received 22 January 2024; Received in revised form 23 May 2024; Accepted 23 May 2024
Available online 23 May 2024

Conclusions: The CM of myocardial motion curves has been associated with LGE infarction, and combining CM with strain features improves the diagnosis of different myocardial LGE infarction degrees.

1. Introduction

Cardiac magnetic resonance (CMR) is the imaging gold standard for monitoring myocardial tissue characteristics and cardiac performance [1]. In myocardial infarction patients, late gadolinium enhancement (LGE) imaging is often combined with cine CMR to identify fibrotic myocardium tissue. LGE images delineate infarcted areas within the myocardium by enhancing the ischemic area with a gadolinium-based contrast agent. However, certain patients, especially those younger or older, and medically ill with impaired breath-holding capacity, compromised kidney function, or allergic reactions to gadolinium-based contrast agents, may be contraindicated for LGE imaging [2]. This challenges the clinical quantification of myocardial fibrosis areas and myocardial infarction diagnosis.

Recently, this issue has garnered the interest of numerous researchers in extracting myocardial motion parameters from cine CMR images to evaluate the degree of myocardial fibrosis and dysfunction. In existing studies, the assessment of myocardial motion has predominantly utilized myocardial strain features. Researchers have extracted the strain and strain rate in the radial, circumferential, and longitudinal directions of the entire heart or specific myocardial segments during myocardial contraction [3,4]. Earlier findings indicated a strong association between myocardial strain characteristics and pathological conditions like hypertrophic cardiomyopathy or myocarditis [5,6]. They have attempted to evaluate myocardial dysfunction using these parameters quantitatively [7]. This study indicates that for myocardium experiencing myocardial infarction, localized myocardial fibrosis may influence strain amplitude and simultaneously affect the motion stability of myocardial segments in different directions. This motion stability can be efficiently evaluated using complexity metrics (CM), a class of features used to gauge the degree of waveform randomness and chaos. These features may provide valuable clinical information about myocardial motion and strain.

Therefore, the main objective of this study was to investigate whether CM extracted from cine CMR can provide additional diagnostic value for patients with myocardial infarction based on traditional segmental myocardial strain parameters. We hypothesized that CM could manifest implicit differences in motion between infarcted and normal myocardium that may go unnoticed by the human eye. When combined with segmental myocardial strain, CM is expected to better assess different degrees of myocardial infarction and help differentiate between different degrees of myocardial infarction assessed by LGE.

2. Materials and methods

2.1. Study group

This retrospective study included myocardial infarction patients who underwent CMR between September 2020 and December 2021. Inclusion criteria were as follows: patients (1) aged between 18 and 90 years and (2) diagnosed with myocardial infarction according to the European Society of Cardiology diagnostic criteria [8] and showed scarring on LGE images. Exclusion criteria were as follows: (1) NYHA cardiac function class III-IV; (2) eGFR $<$30 mL/min/1.73 m^2; (3) patients with other severe cardiomyopathies or cardiac implants including atrial fibrillation, mitral stenosis, or prosthetic valves; (4) contrast allergy; (5) contraindications to MR examination. The study protocol was approved by the hospital ethics committee and complied with the 1975 Declaration of Helsinki guidelines. All patients or their family members signed written informed consent.

2.2. Baseline characteristics

Basic information, history of cardiomyopathy, and vascular risk factors were collected through patient case records. Vascular risk factors collected included hypertension, diabetes, hypercholesterolemia, and smoking history. Hypertension was defined as patients with blood pressure greater than 140/90 mmHg or taking antihypertensive medication. Hypercholesterolemia was defined as patients with low-density lipoprotein cholesterol levels greater than 140 mg/dL, high-density lipoprotein cholesterol levels less than 40 mg/dL, and triglyceride levels greater than 15 mg/dL, or who were being treated with lipid-lowering drugs. Diabetes mellitus was defined as patients with fasting blood glucose greater than 125 mg/dL or HbAlc greater than 6.5 % or who were treated with hypoglycemic drugs. Patients who had smoked in the 12 months before admission were categorized as smokers.

2.3. CMR imaging protocol and analysis

Image acquisition was conducted using an integrated PET/MR scanner (uPMR 790, United Imaging Healthcare, Shanghai, China). CMR was performed utilizing a 12-channel cardiac phased array coil. Imaging was executed by end-expiratory breath-hold and electrocardiography gating. The CMR programs included cine and LGE sequences. Cine CMR sequences were acquired for two-chamber, four-chamber, and short-axis images. The scanning sequence employed a balanced steady-state free-feeding sequence without a contrast agent, with a repetition time and echo time of 3.1 ms and 1.4 ms, respectively, a flip angle of 40°, a matrix size of 288 $\times$ 256, and a scanning time control of 10–15 s at each level.

Based on the cine CMR images in short-axis view, we calculated basic left ventricle (LV) parameters, including LV ejection fraction (%), LV end-diastolic volume index (mL/m^2), LV end-systolic volume index (mL/m^2), and LV mass (g/m^2) in all subjects.

2.4. LGE imaging protocol

LGE imaging was conducted following the completion of cine CMR. The protocol commenced with an intravenous injection of gadopentetate dextran (dose 0.15 mmol/kg, flow rate 2.0 mL/s) and an equivalent saline volume. After waiting 8–10 min, a phase-sensitive inversion recovery sequence scan was performed. The scanning plane and localization of the LGE were consistent with the cine CMR sequence, with a repetition time and echo time of 4.7 ms and 1.9 ms, respectively, a flip angle of 20°, a matrix size of 240 × 180, and an inversion time of 300–330 ms.

2.5. Myocardial segmentation

We segmented the LV myocardium of cine CMR and LGE images in this research. Two professionally trained researchers contoured the LV inner and outer membrane boundaries of the short-axis cine CMR images using the 3D Slicer software (version 5.22 stable release). Despite minimal differences in the contours drawn by the two individuals, calibration was performed to ensure the relative objectivity and accuracy of the data. Based on the mapped LV inner and outer membrane boundaries, we used the criteria specified by the Society for Cardiovascular Magnetic Resonance in 2020 to segment the LV myocardium [1]. Only cross-sectional images containing a full 360° of myocardium were included. After excluding apical segments, the LV was divided into three thick, short-axis planes: basal, intermediate, and apical layers. These three planes were subdivided into six, six, and four segments, yielding 16 myocardial segments according to the segmentation principle.

2.6. Myocardial classification

The infarction areas were manually delineated in the LGE images, and the scar then corresponded to 16 myocardial segments to calculate the transmural extension (TE) for each segment. Based on the value of TE, all myocardium was classified into three groups. Myocardium without any LGE enhancement was defined as remote myocardium (Remote segments); myocardial segments showing 0 % < TE < 50 % were defined as infarcted but viable myocardium (Viable segments), and myocardial segments with a TE > 50 % were defined as nonviable myocardium (Unviable segments) [9].

2.7. Feature extraction

The strain, strain rate, and CM of each myocardial segment were extracted from cine CMR images. This process commenced by obtaining the radial and circumferential lengths of the myocardial segments from the short-axis cine CMR images for every frame, allowing the generation of radial and circumferential motion curves throughout one cardiac cycle. These curves were filtered using wavelet transform, and feature extraction was performed. The strain characteristics of myocardial segments included radial strain,

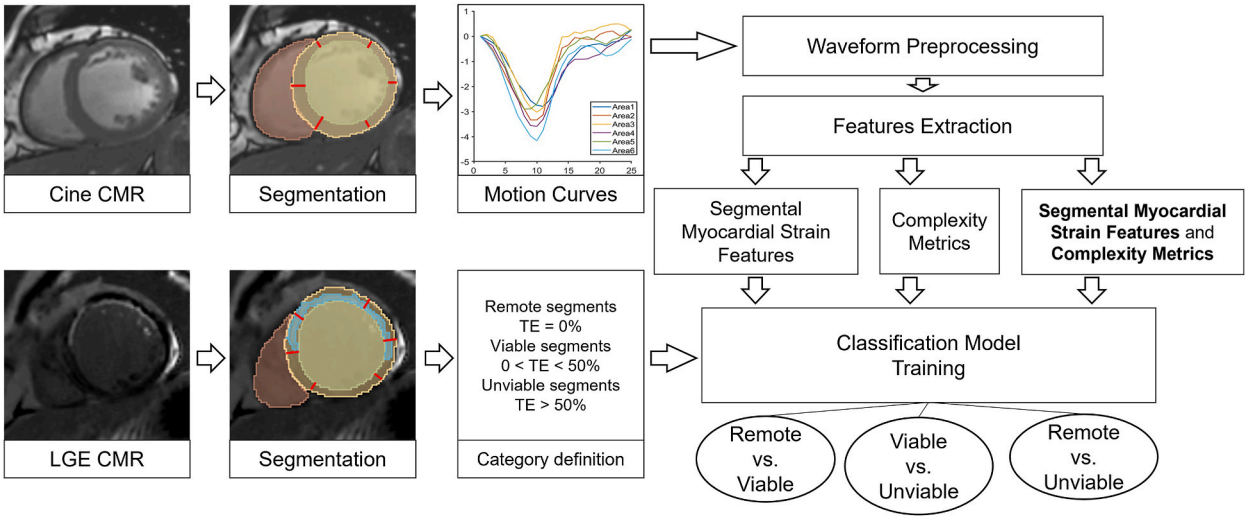

Fig. 1. General methodology diagram based on segmental myocardial strain features and CM approach for distinguishing between remote, viable, and unviable segments. Using LGE as a reference, each segment's TE ratio was computed, serving as the foundation for category definition. Segmental myocardial strain features and CM were extracted from cine CMR images and used to train classifiers to classify myocardial regions with different TE.

radial strain rate, circumferential strain, and circumferential strain rate. For radial and circumferential curves, the CM of myocardial segments comprised frequency drift (FD), power spectral entropy, margin factor, and singular spectrum entropy. Overall, each myocardial segment had four strain parameters along with eight CM.

2.8. Classification

This study assessed the classification performance of CM features by training the machine learning models using various input data, including segmental myocardial strain, CM, or a combined dataset of myocardial strain and CM. The classification effects of these three types of parameters were compared using DeLong's test. The model performed one-to-one classification of remote vs. viable segments, viable vs. unviable segments, and remote vs. unviable segments, respectively. A five-fold cross-validation was employed for iterative training during the model training process.

The classification models were trained using three different algorithms: nonlinear support vector machine (SVM) models, eXtreme Gradient Boosting models (XGBoost), and Neural network models. The study employed the cost-sensitive learning approach [10] with uniform down-sampling to address the issue stemming from the imbalance in the three types of myocardial data.

The general methodology diagram of the model's training process in this study is displayed in Fig. 1.

2.9. Statistical analysis

Continuous variables were expressed as mean ± standard deviation. Kruskal-Walli's test with post hoc Bonferroni test was performed for intergroup analysis. Pearson correlation coefficients were calculated to determine the correlation between CM features and the TE of myocardial segments. Additionally, univariate linear regression analysis was conducted using β values and validated through the F-test. To ensure the validity of our regression analysis, the normality, independence, and homoscedasticity of residuals were assessed using the D'Agostino-Pearson test, Durbin-Watson test, and standardized residual plots, respectively. Multiple linear regression analysis was conducted to assess the independent predictive ability of CMs, with segmental myocardial strain as a covariate. The significance of individual coefficients in multiple regression analysis was tested using T-tests. Collinearity test was assessed via the variance inflation factor (VIF). Moreover, to test each parameter's diagnostic efficacy, we evaluated each feature's classification performance in differentiating three distinct degrees of myocardial infarction. Prior to conducting the aforementioned analysis, all data extracted in this study underwent screening according to the Pauta criterion method (also known as the 3σ criterion).

Receiver operating characteristic (ROC) curves of the validation set results for each classification were generated for the trained SVM, XGBoost, and neural network models. The area under curve (AUC), specificity (Spec), sensitivity (Sens), and accuracy (ACC) were calculated to assess the classification accuracy. Myocardial segmentation, feature extraction, correlation analysis, linear regression analysis and DeLong test were performed using Matlab (version 2018b, The MathWorks Inc, Natick, MA) or MedCalc software (version 20.217, MedCalc Software Ltd, Ostend, Belgium). The machine learning classifiers to distinguish between various types of segments were constructed using Matlab Classification Toolbox (https://michem.unimib.it/download/matlab-toolboxes/classification-toolbox-for-matlab/).

Table 1
Baseline characteristics of the study group and cardiac magnetic resonance parameters.

Characteristics	Myocardial infarction patients N = 42
Baseline characteristics	
Age (years)	60.71 ± 11.23
Male (%)	33 (78.57)
Diabetes mellitus (%)	19 (45.24)
Hypertension (%)	20 (47.62)
Dyslipidemia (%)	9 (21.43)
Current Smoker (%)	27 (64.29)
Heart rate (beats per min)	68.29 ± 10.89
Magnetic resonance parameters	
Stroke Volume (ml)	68.85 ± 17.93
LV Ejection fraction (%)	47.06 ± 14.56
LV End-diastolic volume index (ml/m^2)	85.30 ± 14.56
LV End-systolic volume index (ml/m^2)	50.60 ± 31.21
LV mass (g/m^2)	108.76 ± 30.07
Infarct percent (% of LV mass)	23.62 ± 11.34
Infarct location	
Anterior (%)	20 (48)
Inferior (%)	16 (38)
Other (%)	6 (14)

Continuous variables are expressed as mean ± standard deviation. LV: Left ventricle.

3. Results

3.1. Patient characteristics

Table 1 presents the clinical characteristics and CMR parameters of the individuals. The study comprised 42 patients with myocardial infarction, of whom 33 were men, and the mean age was 60.71 ± 11.23 years. A total of 672 cine CMR sequences of myocardial segments were used for feature extraction, including 208 remote segments (31.0 %), 384 viable segments (57.1 %), and 80 unviable segments (11.9 %).

3.2. Correlation of myocardial features with TE

The correlation between individual myocardial characteristics and the severity of myocardial fibrosis was initially examined. Table 2 illustrates the correlation between strain, strain rate, and CM with TE. Among the segmental myocardial strain characteristics, there was a correlation between radial strain, radial strain rate, and circumferential strain with TE ($r > 0.3$), with a significant negative correlation between radial strain and radial strain rate with TE ($r = -0.496$, $P < 0.001$; $r = -0.528$, $P < 0.001$) and a positive correlation between circumferential strain and TE ($r = 0.327$, $P < 0.001$).

There was a correlation between six features of CM and LGE volume ($r > 0.3$), with the correlation between FD of the radial motion curve and TE being the most pronounced among all CM ($r = 0.496$, $P < 0.001$). At the same time, the results of univariate linear regression analysis shows that the eight CM parameters of radial and circumferential strain all shows significant linear correlation ($P < 0.001$). Among them, six passes the normality test, independence test, and homoscedasticity test of residuals. Furthermore, there was a positive linear correlation between the radial CM and TE, indicating that as the LGE ratio increases, the radial motion complexity increases. Conversely, there was a negative linear correlation between the circumferential CM and TE, indicating that the complexity of circumferential motion decreased with the increase of TE. The findings indicated a significant correlation between CM of myocardial motion and LGE-TE.

We analyzed the diagnostic efficacy of all acquired myocardial features for three different types of segments with different degrees of LGE. Table 2 depicts that the parameter of FD for radial and circumferential motions exhibited good AUC (AUC = 0.65–0.89, AUC = 0.60–0.79), indicating its diagnostic efficacy. CM, other than FD, also showed practical diagnostic efficacy. Significantly, while employing CM to categorize the three types of segments, viable vs. unviable segments (AUC = 0.61–0.78) and remote vs. unviable segments (AUC = 0.71–0.89), all had practical classification efficacy. However, the classification efficacy of the individual CM between remote vs. unviable segments was comparatively less effective (AUC = 0.56–0.68).

The linear regression analysis was performed to assess the autonomous predictive capability of CM, with segmental myocardial strain included as a covariate. The results in Table 2 indicated that, there is no significant collinearity among these parameters (VIF <10). Furthermore, even with segmental myocardial strain considered as a covariate, four CMs retained independent predictive significance ($P < 0.05$). This underscores the continued importance of CMs in assessing myocardial motion, demonstrating their sustained predictive value despite the influence of segmental myocardial strain.

Table 2
Correlation between parameters and myocardial severity and diagnostic performance of parameters.

Features	r [a]	β [b]	P [c]	*AUC*		
				Remote vs. Viable	Viable vs. Unviable	Remote vs. Unviable
Segmental myocardial strain						
Radial strain	−0.496	−0.742		0.68 ± 0.05	0.73 ± 0.06	0.87 ± 0.05
Radial strain rate	−0.528	−0.537		0.68 ± 0.05	0.75 ± 0.06	0.89 ± 0.05
Circumferential strain	0.327	0.194		0.59 ± 0.04	0.66 ± 0.07	0.75 ± 0.07
Circumferential strain rate	0.241	0.405		0.56 ± 0.05	0.63 ± 0.07	0.69 ± 0.05
Complexity metrics						
Radial strain						
FD	**0.496**	0.013†	<0.001	0.65 ± 0.04	0.77 ± 0.05	0.89 ± 0.04
Power spectral entropy	0.376	0.088†	<0.001	0.59 ± 0.05	0.69 ± 0.07	0.78 ± 0.06
Clearance factor	0.443	0.403	0.960	0.68 ± 0.05	0.69 ± 0.05	0.84 ± 0.06
Singular spectrum entropy	0.334	0.258†	0.320	0.67 ± 0.05	0.61 ± 0.07	0.77 ± 0.06
Circumferential strain						
FD	**−0.365**	−0.005†	<0.001	0.60 ± 0.05	0.70 ± 0.07	0.79 ± 0.08
Power spectral entropy	−0.341	−0.098†	0.021	0.58 ± 0.05	0.69 ± 0.07	0.76 ± 0.07
Clearance factor	−0.274	−0.172	0.840	0.59 ± 0.05	0.68 ± 0.05	0.76 ± 0.07
Singular spectrum entropy	−0.240	−0.161†	0.219	0.60 ± 0.05	0.61 ± 0.06	0.71 ± 0.07

FD: Frequency drift. AUC: Area under curve.

[a] Pearson Correlation Coefficient (All $P < 0.001$).

[b] The significance of the regression coefficients was tested using the F-test (All $P < 0.001$). The normality, independence, and homoscedasticity of residuals were assessed using the D'Agostino-Pearson († passes, $P > 0.05$), Durbin-Watson (all passes, 0–4), and standardized residual plots (all passes), respectively.

[c] Multiple linear regression with segmental myocardial strain covariates was analyzed using the T-test. Collinearity assessed via variance inflation factor (VIF) showed no significant collinearity with all VIF <10.

The correlation between FD and TE was most pronounced among all CM features. Fig. 2 illustrates the correlation between FD and TE, along with the normal probability plot of residuals and the residuals equality of variances plot. Fig. 3 shows the differences in FD among myocardial types, and the diagnostic performance of FD. Fig. 2A–C shows that with the increase of TE, there is a statistically significant increase in the FD of radial motion curves ($P < 0.001$), and the residuals satisfies both the normality test ($P > 0.05$) and the homogeneity of variances. Fig. 3A and B illustrate the FD of the radial motion curve, and shows varying severity among the three groups of segments. When radial FD was used for myocardial classification, it demonstrated effective differentiation between remote and unviable segments (AUC = 0.89) and effective between unviable and viable (AUC = 0.77). However, it had marginally inferior performance distinguishing between remote and viable (AUC = 0.65). Fig. 2D–F demonstrate that the circumferential motion curve FD exhibited a negative correlation with TE, and Fig. 3C and D shows varied statistically among the three types of segments. Although circumferential FD exhibited inferior diagnostic performance compared to radial FD, it successfully distinguished remote vs. unviable segments (AUC = 0.79) and viable vs. unviable segments (AUC = 0.70).

3.3. Classification performance

The three types of segments were categorized on a one-to-one basis in this study utilizing multiple machine learning algorithms, and the myocardial strain parameters, CM, and myocardial strain combined CM as inputs to the models. The validation set classification outcomes of the models trained with these three types of parameters are displayed in Table 3. Evidently, the validated AUC of the classification model was lower than that of the myocardial strain parameter (AUC = 0.69–0.90) after training solely with CM (AUC = 0.67–0.89). In contrast, when myocardial strain parameters were trained with CM, the classification model exhibited improved diagnostic performance compared to using only one parameter type as input (AUC = 0.70–0.92). The DeLong test results revealed different ROC curves for combining the two groups of parameters compared to using only segmental myocardial strain parameters ($P < 0.05$), indicating distinct test efficacies. Sensitivities, specificities, and accuracies for all models are given in Table 3.

Fig. 4 depicts the ROC curves of the top three models trained using myocardial strain combined with CM as model input. The results indicated that the classifier could distinguish between remote vs. unviable segments (AUC = 0.92) and viable vs. unviable segments (AUC = 0.78). However, it showed moderate effectiveness in distinguishing between remote and viable segments (AUC = 0.70).

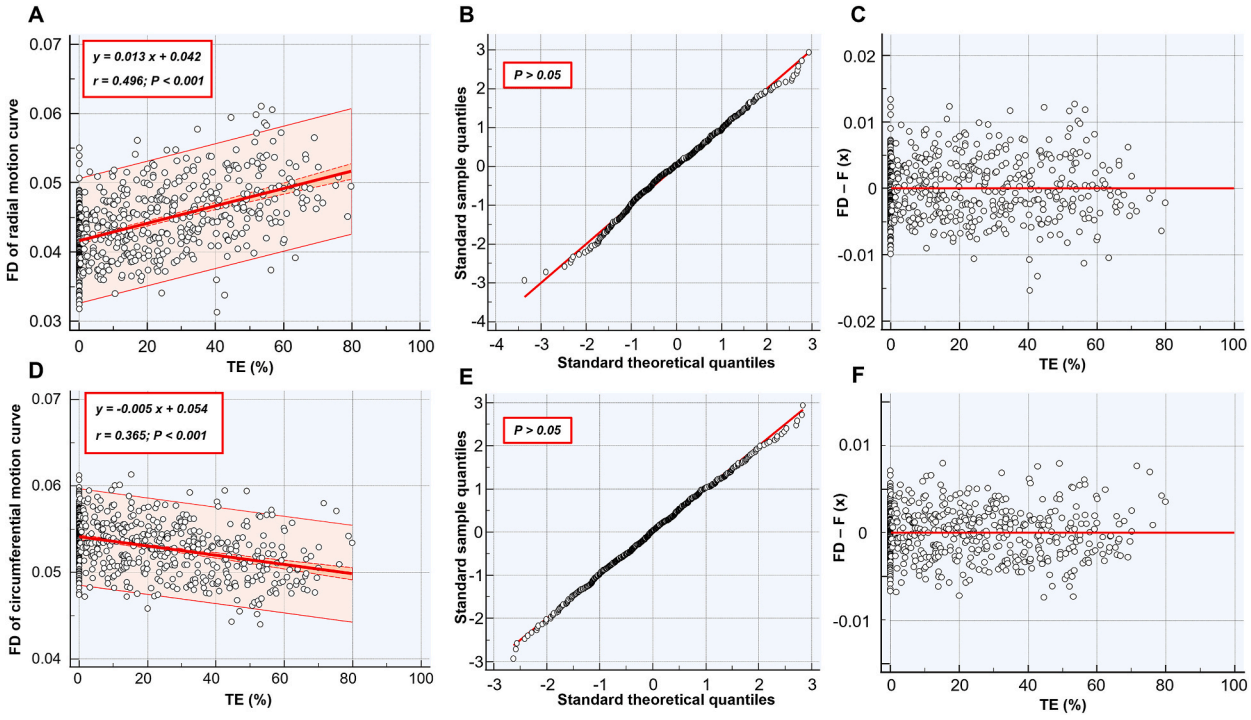

Fig. 2. Linear correlation between FD and LGE TE in myocardial segments. Radial strain FD and TE have a strong positive linear correlation in (A), (B) demonstrates that the residuals of the linear regression analysis satisfy the assumption of normality, (C) shows that the residuals of the linear regression exhibit homoscedasticity. Circumferential strain FD exhibits a negative correlation with TE in (D), along with the (E) and (F) shows that the normality and homoscedasticity of residuals were passed. P-values of (A) (D) were calculated using F-test. P-values of (B) (E) were calculated using D'Agostino-Pearson test.

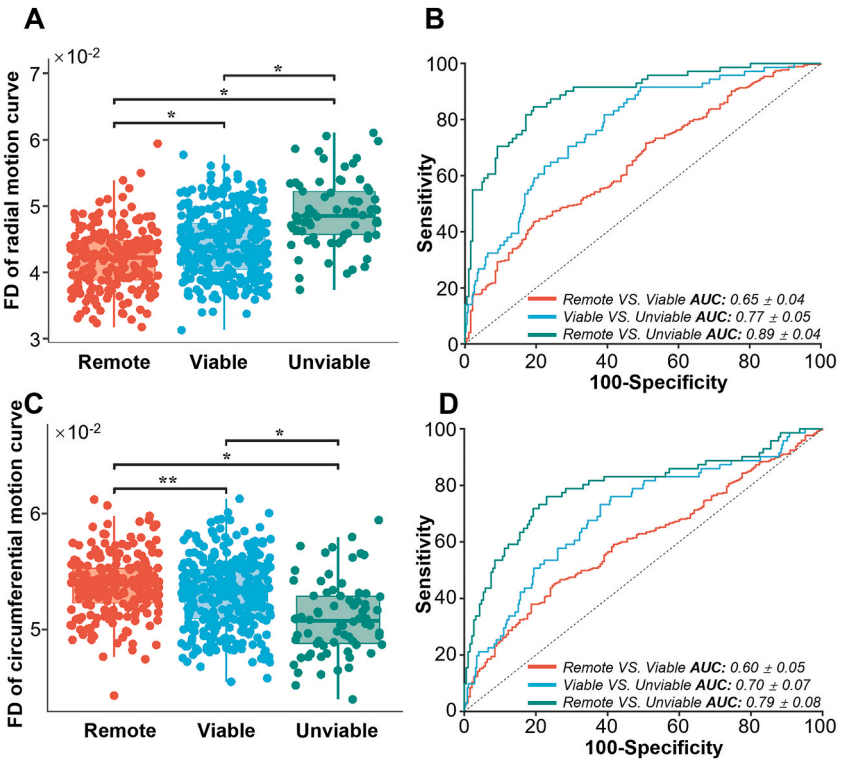

Fig. 3. The intergroup differences and diagnostic performance of FD. (A) illustrates significant variations in radial FD across the three myocardial groups. (B) underscores radial FD's robust diagnostic potential for these myocardial types. (C) points out statistically significant differences in circumferential FD among the three myocardial groups, with (D) emphasizing the diagnostic value of circumferential FD for these groups. The * represents $P < 0.001$, and the ** represents $P < 0.05$. *P*-values were calculated using Kruskal-Walli's test with Bonferroni post hoc.

Table 3
AUC, specificity (%), sensitivity (%), and accuracy (%) of classification models using different inputs.

Models	Remote vs. Viable				Viable vs. Unviable				Remote vs. Unviable			
	AUC	Spec	Sens	ACC	**AUC**	Spec	Sens	ACC	**AUC**	Spec	Sens	ACC
Segmental myocardial strain features												
SVM	0.63	67	62	62	0.70	69	65	66	0.85	85	88	87
XGBoost	**0.69**	68	62	65	**0.75**	74	70	71	**0.90**	90	83	86
Neural network	0.60	63	65	62	0.76	65	73	70	0.89	88	86	87
Complexity metrics												
SVM	0.63	67	62	63	0.70	71	66	67	0.88	86	83	84
XGBoost	0.63	69	56	63	**0.73**	81	68	71	**0.89**[a]	92	86	88
Neural network	**0.67**[a]	64	65	63	0.66	65	65	65	0.86	86	83	84
Segmental myocardial strain features + complexity metrics												
SVM	0.64	66	54	63	0.71	67	70	69	0.89	85	87	86
XGBoost	0.66	66	62	66	**0.78**[a]	79	70	72	**0.92**[a]	89	88	88
Neural network	**0.70**[a]	63	66	64	0.72	76	66	68	0.88	84	83	83

AUC: Area under curve. Spec: Specificity. Sens: Sensitivity. ACC: Accuracy. SVM: Support Vector Machine. XGBoost: eXtreme Gradient Boosting.
[a] ROC curves were statistically significantly different from models with segmental myocardial strain features as input. ($P < 0.05$, by a DeLong test for correlated ROC curves).

4. Discussion

In this research, we extracted CM of myocardial motion curves based on the cine CMR of 42 myocardial infarction patients. We discovered that various CM correlated significantly with myocardial LGE severity; in particular, FD performed exceptionally well in differentiating between myocardium of varying severity. By training machine learning models, it was revealed that classification efficacy may be enhanced by combining segmental myocardial strain with CM, as compared to using just segmental myocardial strain. These findings underscore the potential role of CM in distinguishing between remote, viable, and unviable myocardial segments in cine CMR images, proposing that CM features may be robust, reproducible, and generalizable imaging markers of myocardial fibrosis and

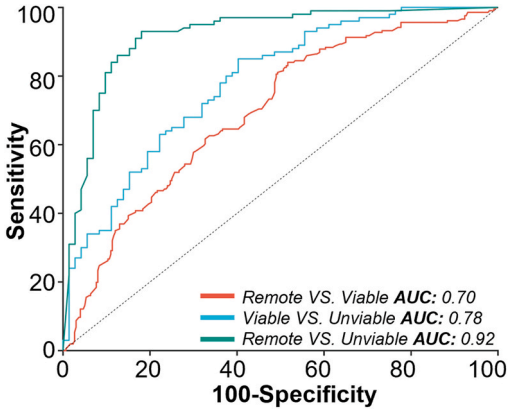

Fig. 4. ROC curves and AUC values of classification models using segmental myocardial strain features and CM as inputs. The model aimed at distinguishing between Remote and Viable myocardium was trained using a Neural network, achieving an AUC of 0.70 (red). The models for differentiating between Viable and Unviable myocardium, as well as between Remote and Unviable myocardium, were trained using the XGBoost algorithm, yielding AUCs of 0.78 (Blue) and 0.92 (Green), respectively.

could potentially offer added value as an incremental parameter in early clinical diagnosis or prognostic follow-up of myocardial fibrosis.

In existing studies, myocardial motion measurement frequently utilizes global and segmental myocardial strains. A combination of these parameters is often employed to diagnose or predict various myocardial diseases, including myocardial fibrosis [11], microvascular obstructions [12], myocarditis [13], and hypertrophic cardiomyopathy [14]. The current investigation emphasizes the significance of motion stability in pathological conditions that induce alterations in myocardial properties, including myocardial fibrosis resulting from myocardial infarction.

The CM is a class of feature values used to assess the degree of randomness and chaos in waveforms, exclusively capturing variations throughout the entire waveform. Distinguishing itself from the majority of parameters, CM exhibits significantly reduced susceptibility to inevitable errors, such as variations in sampling position, thereby exhibiting enhanced stability and reproducibility. It is commonly used in mechanical engineering to evaluate the wear and tear of mechanical equipment or for fault identification [15]. Recently, this class of parameters has garnered the attention of many medical researchers. Some researchers have used the complexity parameters of electromyography to assess the state of human muscles [16]. Others have performed complexity analysis of electroencephalographic signals to monitor emotional states [17] or to diagnose cognitive disorders like epilepsy or depression [18,19]. Zhao et al. and Wang et al. [20,21] identified a substantial correlation between the image entropy of LGE infarct margins and ventricular arrhythmias in cardiovascular imaging. In this study, we calculated the CM of myocardial segmental motion curves and used them to assess myocardial motion stability quantitatively in different directions.

Our results revealed a noteworthy association between CM and myocardial TE, particularly with FD, characterizing the standard deviation of the oscillatory frequency of the motion curve [22]. FD shows a significant linear correlation ($P < 0.001$) with the proportion of scarring, with a correlation coefficient of 0.496. The variations in FD among different severity of myocardium were statistically significant. All other CM demonstrated significant correlation with TE, with six of them passing the normality test, independence test, and homoscedasticity test for residuals. Besides FD, several other CM-TE correlations exceeded 0.3. CM of myocardial motion also had strong diagnostic performance in detecting the severity of LGE in myocardial infarction patients. Moreover, when we combined these two types of parameters as inputs for the classification models, the ROC curves of the models differed from those when only the traditional myocardial strain parameter was used, and the performance of the model was higher than that of the results when the two types of parameters were trained separately. This further validates the diagnostic efficacy of CM and suggests that CM is not a replacement for segmental myocardial strain parameters. In addition, the computational cost of CM features is relatively low. Based on the extraction of motion curves and calculation of myocardial strain features, CM parameters can be extracted with low time consumption. Therefore, we believe it can be a supplementary tool to improve the diagnostic outcomes of segmental myocardial strain parameters.

Notably, the correlation between CM and TE for radial and circumferential motion curves shows an opposite trend. Specifically, radial motion CM increases with increasing myocardial infarction, while circumferential motion CM decreases with increasing myocardial infarction. We speculate that this phenomenon is related to these parameters' scar distribution or physiologic significance. First, radial motion reflects changes in the thickness of the myocardium. The scar distribution is usually heterogeneous when localized infarction occurs in a myocardial segment. This non-uniform distribution can lead to variations in the myocardium's contraction and diastole, which may significantly increase the disorganization of the radial motion curve in the infarcted myocardium. This increased disorganization is reflected in increased complexity with higher TE. In contrast, the circumferential motion of myocardial segments is less affected by scar distribution and mainly reflects changes in the amplitude of myocardial motion. Infarcted myocardium is typically less active due to ischemia, causing smoother motion with less fluctuation in the circumferential motion curve. Consequently, circumferential motion complexity decreases with higher TE. Although the mechanisms mentioned above remain speculative and

await confirmation through future studies, there seems to be a noticeable correlation between the CM and myocardial status, discernible in both radial and circumferential movements.

Based on strain parameters and CM, this study utilized multiple machine learning models to obtain good diagnostic results for LGE ratios of myocardial segments. These models showed excellent performance in distinguishing between myocardial segments with TE > 50 % and TE = 0 % (AUC = 0.92). Additionally, they exhibited good performance in differentiating between myocardial segments with TE > 50 % and those with 0 % < TE < 50 % (AUC = 0.78). An earlier study pointed out that at TE levels >50 %, full recovery of the damaged myocardial segments is difficult even if revascularization procedures are successful [23], highlighting the importance of distinguishing TE > 50 % from other myocardial categories. The models presented in this study are able to automatically differentiate TE > 50 % from the remaining two myocardial categories, solely utilizing cine CMR images without requiring additional LGE imaging. This provides clinicians with invaluable information in a timely manner. However, the diagnostic efficacy of the classifiers was low when differentiating between segments in the remote group with TE = 0 and the viable group segments with 0 % < TE < 50 % (AUC = 0.70). Several factors may be associated: some studies have noted impaired kinetic coordination and synchronization of adjacent myocardial segments in the setting of reduced function in the infarcted region [24]. Others have suggested that it appears normal on LGE images and may have a high degree of extracellular fibrosis [25]. With these effects, it becomes challenging to effectively differentiate between the LGE imaging results of these two types of myocardium, whether by using myocardial strain parameters, CM alone, or combining both types of features. This problem may be alleviated by combining multimodal imaging of the heart and classifying the myocardium at a finer level.

4.1. Study limitations

Certain limitations apply to this study. First, the sample size was relatively small, and the dataset was relatively limited for machine learning models. However, the models were designed to validate the association between CM and LGE, as well as to assess the additional predictive information provided by CM in forecasting LGE. Through a comprehensive consideration of the training results of the machine learning models, correlation analysis, and linear regression analysis, it is sufficient to demonstrate the reliability of the results and key conclusions of this study. Second, manual LV myocardial edge and LGE region segmentation was used. Utilizing existing, mature deep-learning segmentation techniques for myocardial edges could enable automated CM analysis of cine CMR [26]. Moreover, this study exclusively employed short-axis cine images to compute radial and circumferential strains and CM for analysis. Previous studies have shown that segmental longitudinal myocardial strain exhibited inferior diagnostic performance in LGE imaging compared to the abovementioned strain types [24]. In addition, the popularity of CMR scanning is hindered by its high demands for MRI equipment and scanning personnel, which restricts the widespread clinical application of the findings from this study. However, we believe that CM characterization of longitudinal motion curves could offer additional diagnostic information as the principal finding of this research. Additional investigation is warranted in future studies.

5. Conclusion

In this research, we discovered a significant correlation between myocardial segment motion curve complexity and the LGE infarction severity. These CMs, specifically FD, demonstrate strong diagnostic properties and can be combined with segmental myocardial strain parameters as an additional tool to offer a new perspective for clinical diagnosis. Furthermore, the introduction of these CMs present a novel approach for exploring research related to myocardial function, potentially advancing the understanding of cardiac physiology.

Data availability statement

Data associated with our study has not been deposited into a publicly available repository. Data will be made available on request.

Declaration of ethics

The Institutional Ethics Committee of Xuanwu Hospital approved this investigation (ethics approval number LYS2022169, ethics approval date November 14, 2022). Written informed consent was obtained from all the subjects.

CRediT authorship contribution statement

Geng Li: Writing – original draft, Software, Methodology, Formal analysis. **Chong Zheng:** Writing – review & editing, Validation, Investigation, Formal analysis, Data curation. **Yadong Cui:** Writing – review & editing, Resources, Investigation, Data curation. **Jin Si:** Writing – review & editing, Supervision, Investigation, Data curation. **Yang Yang:** Writing – review & editing, Project administration, Conceptualization. **Jing Li:** Writing – review & editing, Project administration, Conceptualization. **Jie Lu:** Writing – review & editing, Validation, Supervision, Project administration, Methodology, Data curation, Funding acquisition, Conceptualization.

Declaration of competing interest

The authors declare the following financial interests/personal relationships which may be considered as potential competing

interests:Jie Lu reports financial support was provided by Ministry of Science and Technology of the People's Republic of China. If there are other authors, they declare that they have no known competing financial interests or personal relationships that could have appeared to influence the work reported in this paper.

Acknowledgments

The authors thank Jie Ma, Hongwei Yang, Dongmei Shuai and Lei Ma for the assistance with the patient studies. This work was supported by National Key Research and Development Program of China (No. 2022YFC2406904) and Huizhi Ascent Project of Xuanwu Hospital (No. HZ2021ZCLJ005).

References

[1] J. Schulz-Menger, D.A. Bluemke, J. Bremerich, et al., Standardized image interpretation and post-processing in cardiovascular magnetic resonance - 2020 update: Society for cardiovascular magnetic resonance (SCMR): Board of trustees task force on standardized post-processing, J. Cardiovasc. Magn. Reson. 22 (1) (2020) 19.
[2] A. Heshmatzadeh Behzadi, M.R. Prince, Preventing allergic reactions to gadolinium-based contrast agents, Top. Magn. Reson. Imag. 25 (6) (2016) 275–279.
[3] J. Xu, W. Yang, S. Zhao, M. Lu, State-of-the-art myocardial strain by CMR feature tracking: clinical applications and future perspectives, Eur. Radiol. 32 (8) (2022) 5424–5435.
[4] M. Kornev, H.A. Caglayan, A.V. Kudryavtsev, et al., Influence of hypertension on systolic and diastolic left ventricular function including segmental strain and strain rate, Echocardiography 40 (7) (2023) 623–633.
[5] F. Wang, X. Xu, Q. Wang, D. Yu, L. Lv, Q. Wang, Comparison of left ventricular global and segmental strain parameters by cardiovascular magnetic resonance tissue tracking in light-chain cardiac amyloidosis and hypertrophic cardiomyopathy, Quant. Imag. Med. Surg. 13 (1) (2023) 449–461.
[6] Q. Gao, W. Yi, C. Gao, et al., Cardiac magnetic resonance feature tracking myocardial strain analysis in suspected acute myocarditis: diagnostic value and association with severity of myocardial injury, BMC Cardiovasc. Disord. 23 (1) (2023) 162.
[7] L.F. Tops, V. Delgado, N.A. Marsan, J.J. Bax, Myocardial strain to detect subtle left ventricular systolic dysfunction, Eur. J. Heart Fail. 19 (3) (2017) 307–313.
[8] K. Thygesen, J.S. Alpert, A.S. Jaffe, et al., Fourth universal definition of myocardial infarction (2018), Eur. Heart J. 40 (3) (2019) 237–269.
[9] V. Bodí, J. Sanchis, M.P. López-Lereu, et al., Usefulness of a comprehensive cardiovascular magnetic resonance imaging assessment for predicting recovery of left ventricular wall motion in the setting of myocardial stunning, J. Am. Coll. Cardiol. 46 (9) (2005) 1747–1752.
[10] X.Y. Liu, Z.H. Zhou, The influence of class imbalance on cost-sensitive learning: an empirical study, IEEE (2006) 970–974.
[11] E. Tahir, J. Starekova, K. Muellerleile, et al., Impact of myocardial fibrosis on left ventricular function evaluated by feature-tracking myocardial strain cardiac magnetic resonance in competitive male triathletes with normal ejection fraction, Circ. J. 83 (7) (2019) 1553–1562.
[12] C. Gräni, A.W. Stark, K. Fischer, et al., Diagnostic performance of cardiac magnetic resonance segmental myocardial strain for detecting microvascular obstruction and late gadolinium enhancement in patients presenting after a ST-elevation myocardial infarction, Front Cardiovasc Med 9 (2022) 909204.
[13] Q. Gao, W. Yi, C. Gao, et al., Cardiac magnetic resonance feature tracking myocardial strain analysis in suspected acute myocarditis: diagnostic value and association with severity of myocardial injury, BMC Cardiovasc. Disord. 23 (1) (2023) 162.
[14] E. Wabich, K. Dorniak, A. Zienciuk-Krajka, R. Nowak, G. Raczak, L. Daniłowicz-Szymanowicz, Segmental longitudinal strain as the most accurate predictor of the patchy pattern late gadolinium enhancement in hypertrophic cardiomyopathy, J. Cardiol. 77 (5) (2021) 475–481.
[15] Q. Jiang, Y. Shen, H. Li, F. Xu, New fault recognition method for rotary machinery based on information entropy and a probabilistic neural network, Sensors 18 (2) (2018) 337.
[16] B.R. Schlink, A.D. Nordin, D.P. Ferris, Human myoelectric spatial patterns differ among lower limb muscles and locomotion speeds, Phys. Rep. 8 (23) (2020) e14652.
[17] A. Tiwari, T.H. Falk, Fusion of motif- and spectrum-related features for improved EEG-based emotion recognition, Comput. Intell. Neurosci. 2019 (2019) 3076324.
[18] S. Raghu, N. Sriraam, Y. Temel, S.V. Rao, A.S. Hegde, P.L. Kubben, Complexity analysis and dynamic characteristics of EEG using MODWT based entropies for identification of seizure onset, J Biomed Res 34 (3) (2019) 1–3.
[19] B. Lord, J.J.B. Allen, Evaluating EEG complexity metrics as biomarkers for depression, Psychophysiology 60 (8) (2023) e14274.
[20] X. Zhao, X. Zhao, F. Jin, L. Wang, L. Zhang, Prognostic value of cardiac-MRI scar heterogeneity combined with left ventricular strain in patients with myocardial infarction, J. Magn. Reson. Imag. 58 (2) (2023) 466–476.
[21] L. Wang, L. Peng, X. Zhao, Y. Ma, F. Jin, X. Zhao, Prognostic value of entropy derived from late gadolinium enhancement images to adverse cardiac events in post-myocardial infarction patients, Acad. Radiol. 30 (2) (2023) 239–247.
[22] V.V. Moca, D. Nikolic, W. Singer, R.C. Mureşan, Membrane resonance enables stable and robust gamma oscillations, Cerebr. Cortex 24 (1) (2014) 119–142.
[23] R.J. Kim, E. Wu, A. Rafael, et al., The use of contrast-enhanced magnetic resonance imaging to identify reversible myocardial dysfunction, N. Engl. J. Med. 343 (20) (2000) 1445–1453.
[24] S. Yu, J. Zhou, K. Yang, et al., Correlation of myocardial strain and late gadolinium enhancement by cardiac magnetic resonance after a first anterior ST-segment elevation myocardial infarction, Front Cardiovasc Med 8 (2021) 705487.
[25] M. Ugander, A.J. Oki, L.Y. Hsu, et al., Extracellular volume imaging by magnetic resonance imaging provides insights into overt and sub-clinical myocardial pathology, Eur. Heart J. 33 (10) (2012) 1268–1278.
[26] L. Xie, Y. Song, Q. Chen, Automatic left ventricle segmentation in short-axis MRI using deep convolutional neural networks and central-line guided level set approach, Comput. Biol. Med. 122 (2020) 103877.